Engineering Failure Analysis xxx (2008) xxx–xxx

Contents lists available at ScienceDirect

Engineering Failure Analysis

journal homepage: www.elsevier.com/locate/engfailanal

Residual stress effects on fatigue life of welded structures using LEFM

Z. Barsoum [a,*], I. Barsoum [b]

[a] Kungliga Tekniska Högskolan (KTH), Department of Aeronautical and Vehicle Engineering, Teknikringen 8, 100 44 Stockholm, Sweden
[b] Kungliga Tekniska Högskolan (KTH), Department of Solid Mechanics, 100 44 Stockholm, Sweden

ARTICLE INFO

Article history:
Received 11 April 2008
Accepted 4 June 2008
Available online xxxx

Keywords:
Welding simulation
FEM
Residual stresses
Fatigue crack growth
Linear elastic fracture mechanics

ABSTRACT

In this paper a welding simulation procedure is developed using the FE software ANSYS in order to predict residual stresses. The procedure was verified with temperature and residual stress measurements found in the literature on multi-pass butt welded plates and T-fillet welds. The predictions show qualitative good agreement with experiments. The welding simulation procedure was then employed on a welded ship engine frame box at MAN B&W. A subroutine for LEFM analysis was developed in 2D in order to predict the crack path of propagating fatigue cracks. The objective was to investigate fatigue test results from special designed test bars from the frame box where all test failed from the non-penetrated weld root. A subroutine was developed in order to incorporate the predicted residual stresses and their relaxation during crack propagation by isoparametric stress mapping between meshes without and with cracks, respectively. The LEFM fatigue life predictions shows good agreement with the fatigue test result when the residual stresses are taken into account in the crack growth analysis.

1. Introduction

Residual stresses are present in many fabricated structures due to local plastic deformation from thermal and mechanical operations during the manufacturing. The presence of residual stresses in engineering components and structures can significantly affect the fatigue behaviour during external cyclic loading. The effect of residual stresses may either be beneficial or detrimental, depending on magnitude, sign and distribution of the stresses with respect to the load-induced stresses. Residual stresses in tension are detrimental and are often in the magnitude of the materials yield strength. The tensile residual stresses will reduce the fatigue life of the structure by increasing the growth of the fatigue crack, while compressive residual stresses will decrease fatigue crack growth rate.

Accurate and reliable residual stress prediction and measurements are essential for structural integrity and fatigue assessment of components containing residual stresses. Simulation of the manufacturing process (e.g. welding and cold working) using finite element technique is an accepted method for predicting the residual stresses. However, finite element simulation of residual stresses due to welding involves in general many phenomena, e.g. non-linear temperature dependent material behaviour, 3D nature of the weld pool and the welding processes and microstructural phase transformation. Despite the simplification by excluding various effects, welding simulations is still CPU time demanding and complex. Hence, simplified 2D welding simulation procedures are required in order to reduce the complexity and thus maintain the accuracy of the residual stress predictions. However, the residual stress distribution for a complex welded structure is usually not known and conservative assumptions are made of the residual stress distribution when linear elastic fracture mechanics (LEFM) fatigue life predictions are carried out [1,2].

* Corresponding author.
E-mail addresses: zuheir@kth.se (Z. Barsoum), imad@kth.se (I. Barsoum).

1350-6307/$ - see front matter © 2008 Elsevier Ltd. All rights reserved.
doi:10.1016/j.engfailanal.2008.06.017

LEFM is frequently employed for fatigue assessment of cracks and flaws in critical welds. In cases when the residual stress distribution is known its effect could be incorporated into the LEFM fatigue life estimation by applying the distribution as a static internal load on the un-cracked component using the weight function method [3] for calculation of the stress intensity factor, K_I. These weight function techniques are limited to basic geometry cases and are out dated. However, Finite element techniques are more general.

The initial residual stresses are redistributed during fatigue crack growth and this effect is incorporated in the developed subroutine for LEFM fatigue life assessment. The work within this paper is divided into five different steps:

1. Development of a FE subroutine for welding simulation procedure in order to predict the residual stresses due to the welding process.
2. Development of a LEFM subroutine for automatic simulation of fatigue crack propagation in order to predict the crack path and to calculate the stress intensity factors (K_I and K_{II}) and the crack deflection angle (φ_i).
3. Development of a subroutine for incorporation of the simulated residual stresses into the LEFM based crack propagation analysis in order to take account of the residual stress redistribution effects into the fatigue life assessment.
4. Validation of the subroutines with experimental and numerical data found in the literature.
5. Implementation of the developed subroutines for the fatigue assessment of a real application welded structure.

Finite element simulations in order to predict temperature fields, residual stresses and deformation due to welding in 2- and 3-dimensional is used more frequently nowadays [4–6]. Also 2D and 3D LEFM fatigue crack growth simulators have been developed [7–9] in order to predict the fatigue life for, i.e. welded joints [9]. There are several research contributions [2,10–12] on the incorporation of residual stress into the fracture mechanical defect assessment. However, limited work has been done on the development of reliable simulation tool in order to include all these features in the same package.

2. Welding simulation procedure

2.1. Finite element modelling

The welding simulation procedure is developed in the FE software ANSYS [13]. The purpose of the welding simulation procedure is to predict temperature, HAZ weld penetration and residual stresses due to welding with simplified 2D welding simulations. A sequentially coupled analysis is carried out starting with the thermal analysis. The results from the thermal analysis – the temperature distributions, were used as loads in the elastic–plastic mechanical analysis. Generalized plane strain was assumed for the FE models, i.e. the strain in the longitudinal welding direction is constant ($\varepsilon \neq 0$) unlike the plane strain condition where the strain is zero ($\varepsilon = 0$). The addition of weld filler material is simulated by using the birth/death of elements in ANSYS for the thermal transient analysis and the elastic–plastic analysis, respectively.

2.2. Heat source modelling

The temperature distribution in a weldment is mainly determined by the gross heat input, the pre-heat temperature, the welding process, type and geometry of the joint [14].

The heat source used in this study assumes a constant distribution of volume heat flux over the cross section of the weld filler material. The volume flux is applied simultaneously with the reactivation of the elements representing the weld filler material with a pre-heating melting temperature (1500 °C). The principal parameter of the welding heat source for the temperature field is heat flow Q_{tot} (J/s) which can be expressed as,

$$Q_{tot} = \eta_{arc} U \cdot I, \tag{1}$$

where η_{arc} – arc efficiency, which account for radiative and other losses from the arc to the ambient environment, i.e. it is assumed that some portion of the energy $(1 - \eta_{arc})$ leaving the electrode never reach the melt pool surface.

U – arc voltage

I – arc current.

The equivalent heat input can be assumed as the combination of prescribed pre-heat temperature, surface and volume heat flux components [15]. Therefore, the total heat input can be written as

$$Q_{tot} = Q_{surface} + Q_{volume} + Q_{filler}, \tag{2}$$

where $Q_{surface}$ and Q_{volume} indicate heat contents resulting from a specific surface heat flux and volume heat flux, respectively. The Q_{filler} indicate heat content resulting from the prescribed preheating temperature. The specific surface heat flux (area-specific heat flow density) $q_{surface}$ (J/mm^2 s) and specific volume heat flux (volume-specific heat flow density) q_{volume} (J/mm^3 s) can be expressed by

$$q_{surface} = \frac{Q_{surface}}{S}, \quad q_{volume} = \frac{Q_{volume}}{V}, \tag{3}$$

Please cite this article in press as: Barsoum Z, Barsoum I, Residual stress effects on fatigue life of welded structures using LEFM, Eng Fail Anal (2008), doi:10.1016/j.engfailanal.2008.06.017

where S is the surface area and V is the volume of weld filler material, respectively. The ratio of $Q_{surface}/Q_{volume}$ and Q_{volume}/Q_{filler} can be tuned to achieve an accurate representation of the fusion zone. In the present study the surface heat flux is ignored and the equivalent heat input, Q_{tot}, is a combination of Q_{volume} and Q_{filler}, i.e. the tuning is restricted to Q_{volume}/Q_{filler}.

There are two approaches to tune a simplified heat source model described above:

- When experiment data is available, "tuning" is accomplished by bringing the calculated temperature histories into agreement with those experimental data measured by the thermocouples.
- When there is no experiment data available, "tuning" means adjusting the weld parameters to achieve a reasonable molten zone size and distance to the HAZ (800–900 °C) from the fusion zone boundary. A reasonable molten zone size is achieved when at least the melting temperature (1340–1390 °C) is reached in all the elements that are included in the particular weld pass.

In the present study the both approaches are utilized in order to predict the fusion zone, HAZ and weld depth penetration with the heat source model described above.

2.3. Material modelling

Accurate material data in the high temperature region is in general difficult to obtain and becomes at best a reasonable approximation. However, the material model and relevant properties need only to represent the real material behaviour with sufficient accuracy.

The material of the weld metal, HAZ and the base metal are assumed to be the same. The material considered is mild steel with the grade of steel ST37-2 [16]. The thermal and mechanical material properties are illustrated as function of temperature in Fig. 1. The stir effect caused by the fluid flow in the molten weld pool has been modelled by applying a thermal conductivity of 300 W/m °C above the melt temperature [17]. The largest effect of transformations in mild steels is the solid

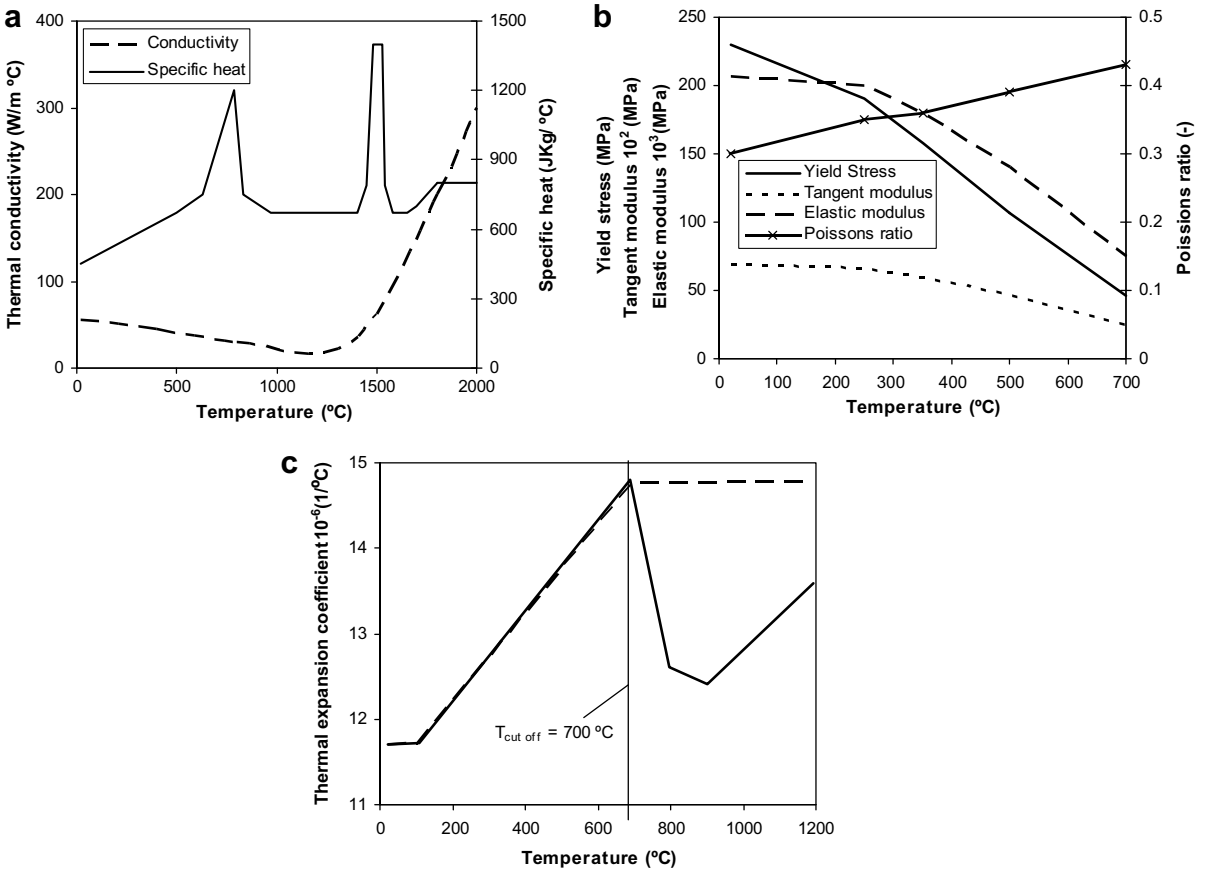

Fig. 1. Material model used for the welding simulations: (a) conductivity and specific heat; (b) yield stress, tangent modulus and elastic modulus and (c) thermal expansion coefficient.

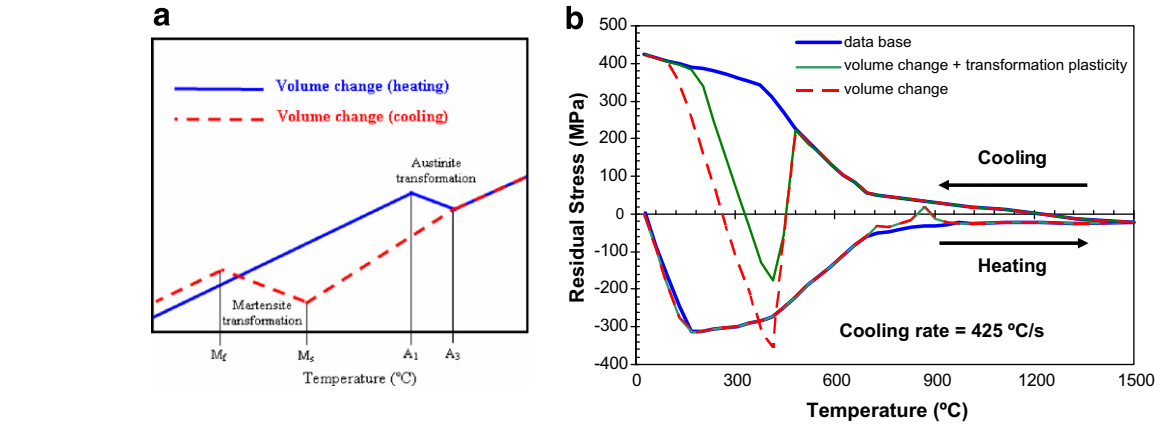

Fig. 2. Effect of phase microstructural transformation on formation of residual stress: (a) schematic diagram of volume change due to phase transformation and (b) influence of volume change, transformation plasticity and base data during heating and cooling, after [20].

phase transformation by austenite decomposition at 700 °C. The latent heat in the solid phase transformation and the solid–liquids phase transformation at the melting point (1480–1530 °C) are included in the heat capacity curve, see Fig. 1a.

The mechanical material properties as function of temperature are shown in Fig. 1b and c. The material model is elastic–plastic with linear kinematic hardening. For typical carbon steels the yield stress is considerably reduced for temperature above 800 °C and naturally vanishes at the melting temperature. The high temperature range, $T \geqslant 0.5^{*} T_{\text{melting}}$, is of little significance for the formation of residual stresses because of the disappearing yield limit in this range [18]. Therefore, a cut-off temperature of 700 °C is used in the mechanical material model, i.e. if the temperature from the thermal analysis is higher than 700 °C then material properties are evaluated at the cut off temperature.

The thermal expansion coefficient as function of temperature for low-alloy steels including the phase transformation from ferrite to austenite at 700 °C is shown in Fig. 1c as a solid line. This is analogous to the specific heat in thermal material model, Fig. 1a. Hansen [19] compared the significances of including this phase transformation in thermal expansion curve and by assuming constant coefficient for temperatures above 700 °C for mild steel. This resulted in no noticeable effect on the residual stress calculations. The dashed line for thermal expansion coefficient in Fig. 1c is used in the present study.

Goldak [20] recommend the following guidelines for the significant effect of microstructure on residual stress formation:

- High yield strength.
- If the phase transformation temperature is close to room temperature.
- If the volume change is large due to the phase transformation.

In low alloy low strength steels with fairly high weld power, the transformation of austenite is usually to ferrite/pearlite and that occurs above 500–600 °C, the yield stress is low, the volume change is small and the transformation temperature is high. The transformation temperature means that plastic deformation after the phase transformation is assumed to erase the memory of the phase transformation, see Fig. 2.

The effect of transformation plasticity on heating around 870 °C is very small. The effect of transformation plasticity on cooling around 250 °C is very large but there is no effect on residual stress at room temperature, 25 °C. If the transformation on cooling had occurred near room temperature, the residual stress would have been compressive. No transformation plasticity is considered in the present work.

3. Validation of welding simulation procedure

The validation of the developed welding simulation procedure is carried out on a single pass butt weld, a two pass butt weld and a T-fillet weld, respectively. The results are compared with predicted and measured temperature and residual stresses found in the literature.

3.1. Butt welded plates

Hansen [19] carried out comprehensive welding simulation, temperature and residual stress measurements on butt welded plates with detailed documentation. The welding was carried out using submerged arc welding. Fig. 3 shows a schematic illustration of the butt welded plates and location temperature measurements and residual stress measurements.

The results form the thermal analysis for the one and two pass butt welded plates are presented in Figs. 4 and 5, respectively. The weld fillers are deposit initially stress free with prescribed melting temperature and heat distribution. The

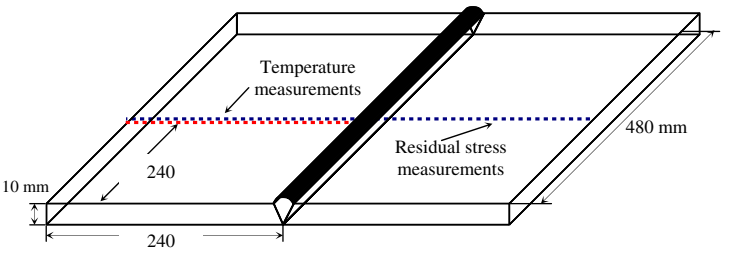

Fig. 3. Schematic illustration of the butt welded plates used in the validation of the welding simulation procedure.

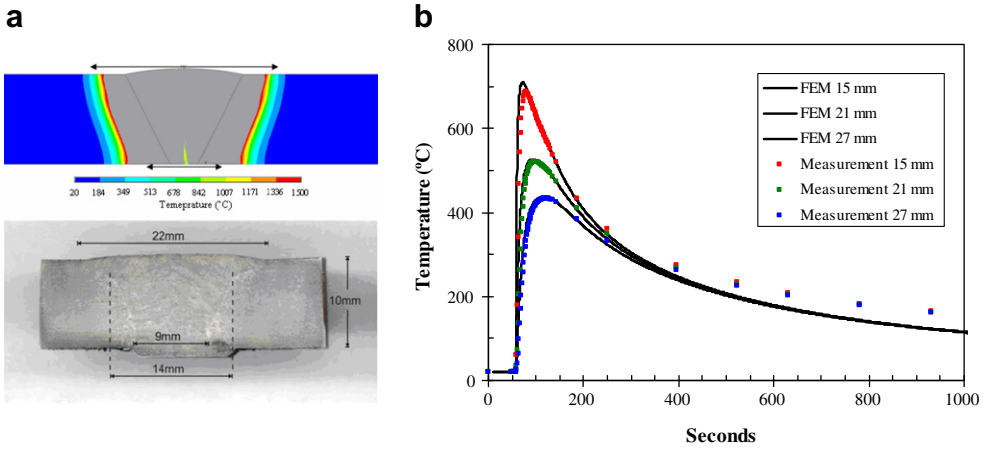

Fig. 4. Thermal analysis of one pass butt welded plate: (a) fusion zone and isotherms and (b) transient temperature curves as function of time.

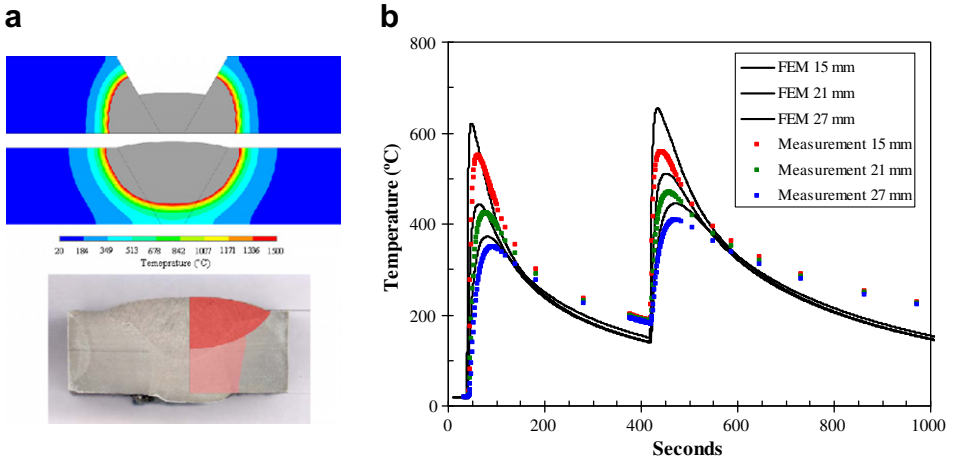

Fig. 5. Thermal analysis of two pass butt welded plate: (a) fusion zone and isotherms and (b) transient temperature curves as function of time.

welding simulation starts with the root pass and continue to build up pass after pass. The isothermal contour plots for the fusion zone, HAZ and penetration profile shows qualitative good agreement with the micro samples. The temperature curves at 15, 21, and 27 mm from the weld centre line shows good agreement with the temperature measurements carried out in Hansen [19]. However, the predicted peak temperatures in the two pass butt welded plate are slightly higher than the measurements.

The results from the mechanical analysis for the one and two pass butt welded plates are presented in Figs. 6 and 7, respectively. The longitudinal residual stresses at the vicinity of the weld in Figs. 6a and 7a shows good agreement with the neutron diffraction measurements and the 3D FE simulation carried out in Hansen [19]. However, the longitudinal resid-

Please cite this article in press as: Barsoum Z, Barsoum I, Residual stress effects on fatigue life of welded structures using LEFM, Eng Fail Anal (2008), doi:10.1016/j.engfailanal.2008.06.017

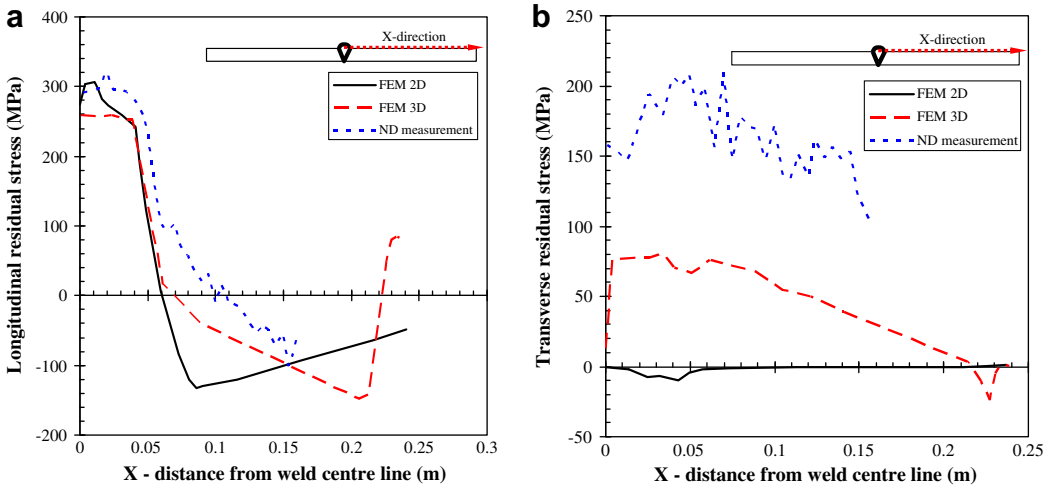

Fig. 6. Residual stress prediction and measurements for one pass butt welded plate: (a) longitudinal residual stresses and (b) transverse residual stresses.

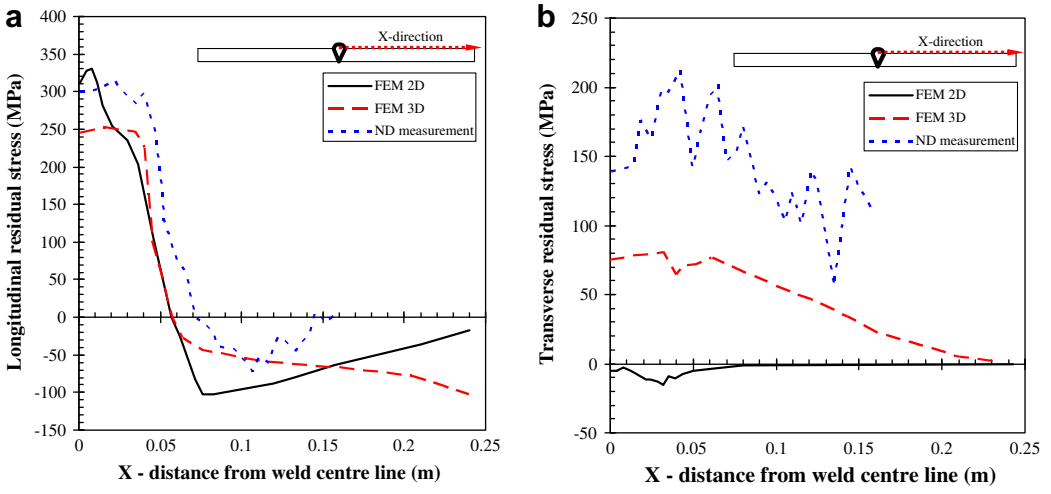

Fig. 7. Residual stress prediction and measurements for two pass butt welded plate: (a) longitudinal residual stresses and (b) transverse residual stresses.

ual stresses at the end of the base plate shows higher residual stresses in the 3D FE simulation. Hansen carried out simulation of the flame cutting process of the end of the base plates, which is included in the 3D welding simulation in Fig. 6. This explains the difference between the 3D and the 2D residual stress predictions at the end of the base plates.

The measured transverse residual stresses are approximately 100–200 MPa and the predicted transverse residual stresses are about 0 MPa. There is no external restraint on the plates and no constraints are able to be build-up in the transverse direction. The transverse residual stresses are better captured with the 3D FEM model, illustrating the 3D nature of the welding process.

Fig. 8 shows the variation of the transverse residual stress along the plate at the vicinity of the weld for a butt welded plate. However, from a fatigue point of view; the transverse residual stresses, e.g. near the weld toes, have a large effect on fatigue cracking. Hence, 3D FEM model or highly constraint 2D models have to be utilized in order to predict the transverse residual stresses accurately for butt welds.

3.2. Fillet welded plates – T-weld

Ma et al. [22] carried out comprehensive FEM analysis of 3D and 2D welding residual stress in T-type fillet welds in mild and high strength steels. The material model assumes temperature dependent of the yield stress and elastic modulus and constant thermal expansion and Poisson's ratio. In the present analysis the previous defined material model and heat source model is utilized. Fig. 9 shows the transient thermal analysis and the dimension of the T-fillet weld analyzed. The two welds are simultaneously welded with the same welding conditions.

Please cite this article in press as: Barsoum Z, Barsoum I, Residual stress effects on fatigue life of welded structures using LEFM, Eng Fail Anal (2008), doi:10.1016/j.engfailanal.2008.06.017

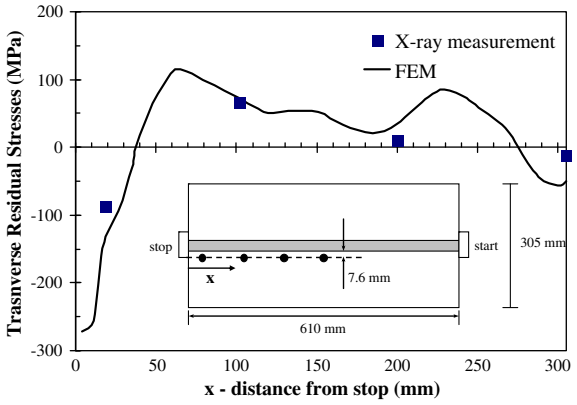

Fig. 8. Transverse residual stress along the weld length for a butt welded plate, after [21].

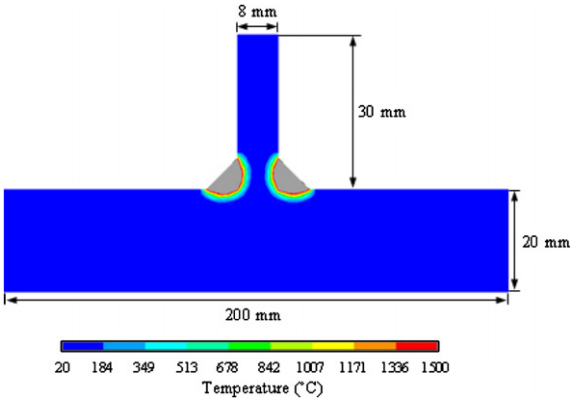

Fig. 9. Thermal analysis, fusion zone and isotherms of simultaneous welding of T-fillet weld.

Fig. 10 shows the longitudinal and transverse residual stresses predicted using the present model. These are compared with the 2D and 3D residual stress predications carried out by Ma et al. [13]. The predicted residual stresses in the present study show very good agreement. The transverse residual stress is also accurately predicted in the T-fillet welds.

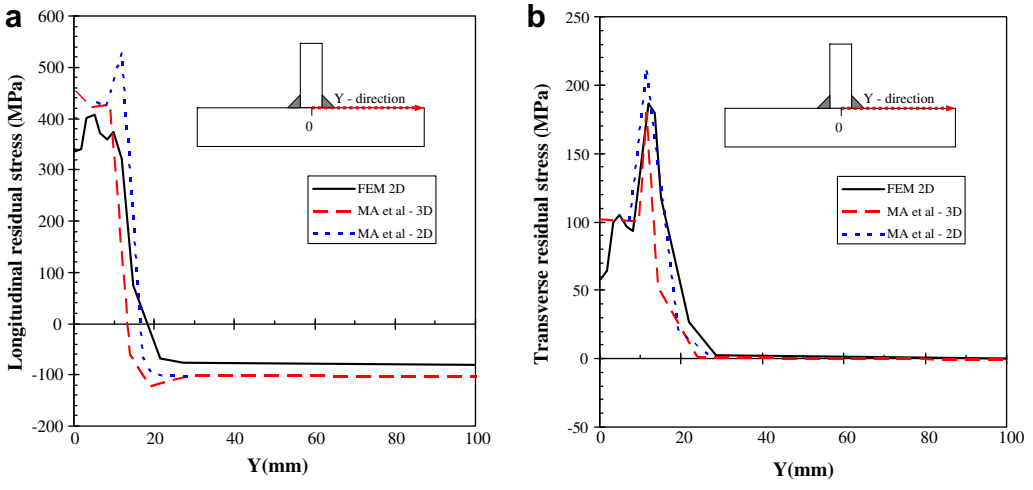

Fig. 10. Residual stress prediction and comparison with Ma et al. [22] for T-fillet weld: (a) longitudinal residual stresses and (b) transverse residual stresses.

Fig. 11 shows that the transverse and longitudinal residual stresses are uniformly distributed along the welding direction in the 3D welding simulation, except the stresses at the weld start and stop position. Hence, simplified 2D generalized plane strain models for residual stress prediction in fillet welds are a good approximation of the 3D nature of the welding process.

4. LEFM fatigue crack propagation simulation

The LEFM fatigue crack growth (FCG) routine is developed in ANSYS. The input for the subroutine is the FE model, crack length and crack growth increment. It is possible to analyze several cracks in the structure and the crack growth increment could be variable, i.e. different crack growth increment during the crack propagation. Fig. 12 shows an illustration of the crack growth implemented in the program. The output is the stress intensity factors (ΔK_I, ΔK_{II}), the crack deflection angle (φ_i) and the fatigue life consumed (ΔN_i) for each specified crack growth increment (Δa_i). ANSYS uses crack tip elements with ¼-point nodes together with crack tip displacement technique for K_I and K_{II} determination. The 2D linear-elastic Mode I/II interaction criteria for numerical computation of incremental crack growth employed is the maximum circumferential stress criterion ($\sigma_{\theta max}$). The $\Delta\sigma_{\theta max}$ theory states that the crack will grow in the direction of maximum circumferential stress at the crack tip [23]. The crack deflection angle, φ, between the crack extension and the crack front under mixed mode is,

$$\varphi = 2\arctan\left(\frac{K_I}{4K_{II}} \pm \frac{1}{4}\sqrt{\left(\frac{K_I}{K_{II}}\right)^2 + 8}\right). \tag{4}$$

Other Mode I/II interaction theories are the maximum potential energy release rate ($G_{\theta max}$) and the minimum strain energy density ($U_{\theta min}$) [24–25]. Bittencourt et al. [8] showed that if the crack orientation is allowed to change in automatic crack growth simulations, the three interaction theories provide basically the same results.

The crack propagation law used is Paris law for stable crack growth together with the IIW recommendations [26] for crack growth parameters, $C = 4.75 \times \cdot 10^{-12}$ MPa $\sqrt{m}$ and m-slope = 3, for 50% failure probability.

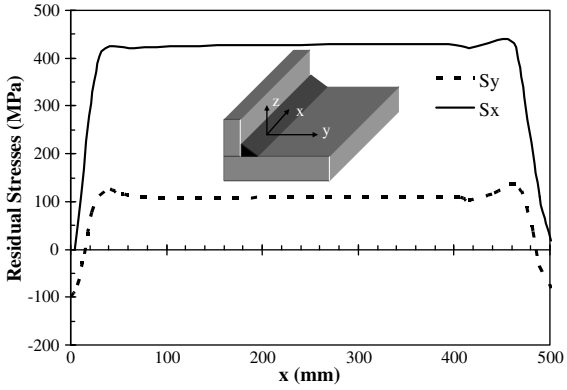

Fig. 11. Residual stresses on the surface of a T-fillet weld showing constant distribution along the welding direction except for the start and stop, after Ma et al. [22].

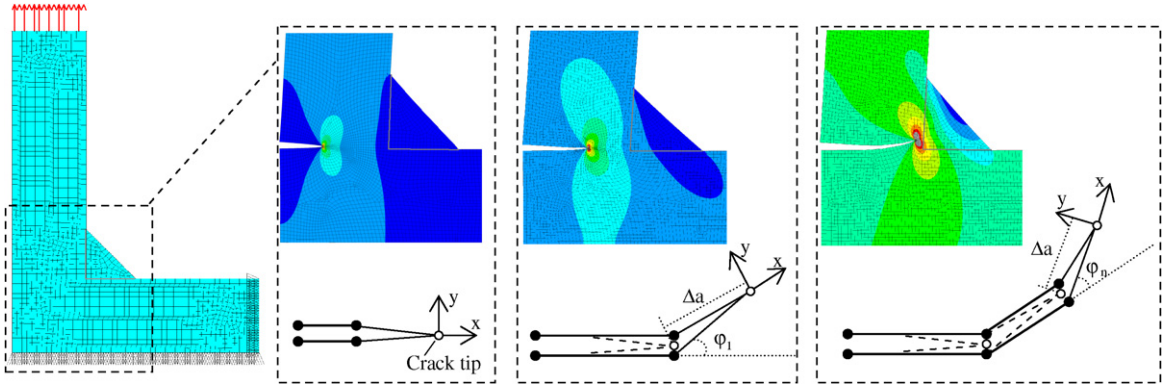

Fig. 12. Modelling of crack propagation and crack deflection in the developed LEFM crack growth simulator. Illustration example; fatigue crack propagation from crack emanating from the weld root in a load carrying fillet welded joint.

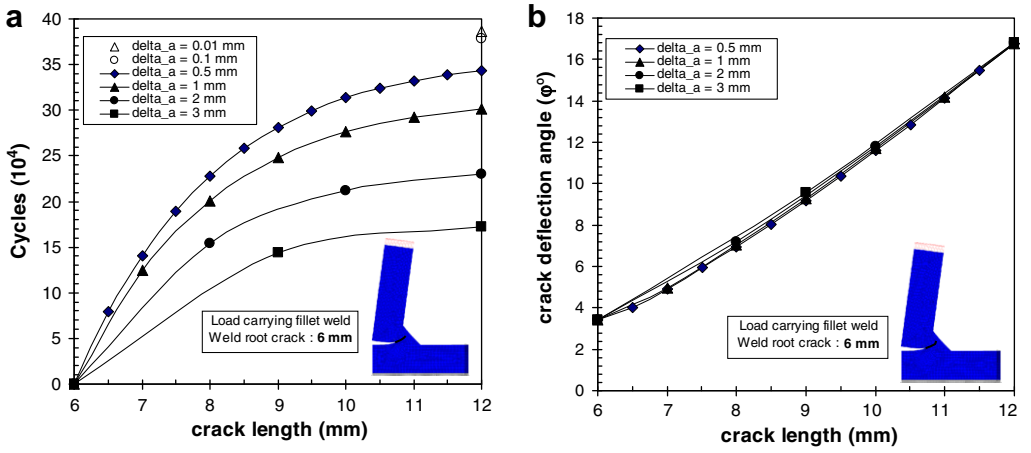

Fig. 13. Effect of crack growth increment: (a) on predicted fatigue life and (b) on crack deflection angle.

Fig. 13 shows the effect of decreasing the crack growth increment (Δa) on the predicted fatigue life (N_f) and the crack deflection angle (φ) using the LEFM FCG subroutine. The analysis was carried out on a 6 mm initial weld root crack propagating 6 mm in a fillet weld, Fig. 12. No residual stresses were considered in this analysis, the material considered was structural steel and the remote loading was $\Delta\sigma_{applied}$ = 120 MPa.

The crack growth increments studied were; 0.5, 1, 2 and 3 mm. It is noticed that the choice of the crack growth increment is most likely affecting the prediction of the fatigue life and reaching an asymptotic value at infinitesimal crack growth increment. Although the predicted crack deflection angle is not affected by the crack growth increment. Rough curve fitting shows that an asymptotic theoretical final fatigue life ($N_f = 3.86 \times 10^4$) is reached for crack growth increment 0.1 mm. However, Δa = 0.5 mm, is used for further analysis in order to reduce the computational time.

5. Incorporation of residual stresses

A quantitative assessment of the influence of the residual stresses on the LEFM fatigue life prediction can be made by the principle of superposition based on the effective stress intensity factor (K_{eff}) as

$$K_{eff} = K_{applied} + K_{residual}, \tag{5}$$

where $K_{applied}$ is the stress intensity factor due to the external applied cyclic loading and $K_{residual}$ is the stress intensity factor due the residual stress. The stress intensity factor, $K_{residual}$, is usually obtained by using weight function solution [3] by applying the residual stress field on the un-cracked component. However, this weight function technique gives only qualitative results for structures that are not according with elementary cases. In order to achieve a more accurate determination of $K_{residual}$ the residual stress distribution has to be known at each stage of the crack growth [27].

5.1. Mean stress approach

The incorporation of residual stresses using the mean stress approach poses that the range of effective stress intensity factor, ΔK_{eff}, does no change when the residual stresses are super-imposed;

$$\Delta K_{eff} = \left(K^{max}_{applied} + K_{residual}\right) - \left(K^{min}_{applied} + K_{residual}\right) = K^{max}_{applied} - K^{min}_{applied} = \Delta K_{applied}. \tag{6}$$

However, the local stress ratio R_{eff} will continually change as the crack propagates trough the superimposed residual stress field for a constant R-ratio, and hence will cause a mean stress alteration at the crack tip as

$$R = \frac{K^{min}_{applied}}{K^{max}_{applied}}, \quad R_{eff} = \frac{K^{min}_{eff}}{K^{max}_{eff}} = \left(\frac{K^{min}_{applied} + K_{residual}}{K^{max}_{applied} + K_{residual}}\right), \quad R_{eff} \neq R. \tag{7}$$

This indicate that the models for crack growth in the residual stresses should include the effective stress ratio in addition to the stress range, i.e. the Forman equation [28];

$$\frac{da}{dN} = \frac{C(\Delta K)^m}{(1 - R_{eff})} \quad \text{for } R > 0 \tag{8}$$

$$\frac{da}{dN} = \frac{C(\Delta K_{eff})^m}{(1 - R_{eff})} \quad \text{for } R < 0 \tag{9}$$

Please cite this article in press as: Barsoum Z, Barsoum I, Residual stress effects on fatigue life of welded structures using LEFM, Eng Fail Anal (2008), doi:10.1016/j.engfailanal.2008.06.017

The mean stress approach is implemented in the weight function LEFM software AFGROW [3] which will not change ΔK_{eff}, but will change the stress ratio (R_{eff}), and will result in a change in the crack growth rate.

5.2. Crack closure approach

The superimposed residual stress intensity factor, K_{residual}, can either decrease or increase K_{eff} depending on the sign of K_{residual} and the crack can only propagate if the crack tip experiences tensile mode-I condition, i.e. $K_{\text{eff}} > 0$. Considering constant R-ratio, only part of the crack will be open if $K_{\text{eff}} > 0$ and closed if $K_{\text{eff}} < 0$. In comparison with the mean stress approach, the crack closure approach can take into account the compressive residual stresses. The fatigue crack growth simulator Franc2D [7] incorporate the residual stress by implementing the crack closure approach. However, no redistribution of the residual stress field is considered in Franc2D during the crack propagation.

6. Residual stress mapping

The welding simulation procedure uses a relatively coarse mesh in comparison to the LEFM FCG subroutine. Also different material models are used; elastic–plastic in the weld simulation procedure and linear elastic in the LEFM FCG subroutine, respectively. In order to incorporate the predicted residual stresses into the crack growth analysis it is necessary to employ a stress mapping algorithm from the old to the new mesh.

ANSYS allows the user to specify initial stress as a loading in a structural analysis which can be specified at the centroid of each element or at the element integration point for each element. When the residual stress field is applied by the ISFILE command an equilibrium calculation step with no additional load and boundary conditions applied is necessary in order to retain the original residual stress field.

The residual stress mapping algorithm is written in MATLAB and is based on inverse isoparametric mapping. This procedure gives an accurate way of mapping the residual stresses from an old mesh to a new mesh when remeshing is made due to crack propagation. The location of a new node n with respect to local coordinate system of the elements in the old mesh can be determined by using the method proposed by Benson [29]. First the node p, belonging to the old mesh, closest to the node n, belonging to the new mesh, is determined. Before remeshing is made a list of elements surrounding each node is generated, which can be obtained from the node connectivity data. Then the closest node p in the old mesh to the specified node n in the new mesh is determined by searching for the smallest distance between the nodes of the old mesh and node p in the new mesh. The list of elements surrounding the closest node provides an initial list of elements that could contain the specified point. The element list will have a maximum of four elements. A vector $\mathbf{s}$ from p to n is then compared with the vectors $\mathbf{v}_1$ and $\mathbf{v}_2$ from p to the two neighbouring nodes along the edges of the same element, as illustrated in Fig. 14. For 8-noded quadratic isoparametric elements the vectors $\mathbf{v}_1$ and $\mathbf{v}_2$ reach the midside nodes of the element. For the node n to be located within the actual element equation 10 must be fulfilled.

$$(\mathbf{v}_1 \times \mathbf{s}) \cdot (\mathbf{s} \times \mathbf{v}_2) \geqslant 0. \tag{10}$$

Among the elements fulfilling this criterion the actual element is found by determining the local coordinates ξ_n and η_n of the node n. If they fall within the range $-1 \leqslant \xi, \eta \leqslant 1$, the specified point will lie within the element. The local coordinates are determined by solving a second order equation defined by the shape functions of the elements. The global coordinates of the nodes of an element in the old mesh passing the criterion in Eq. (10) are denoted x_i and y_i and the global coordinates of the new node n are denoted x_n and y_n. Hence the local coordinates ξ_n and η_n of the node n can be determined by solving

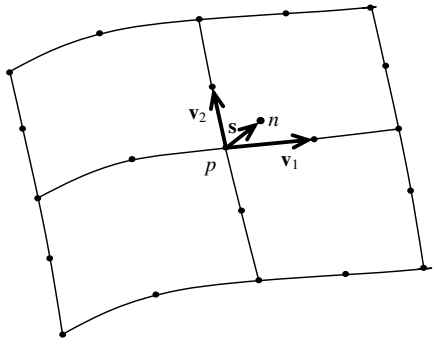

Fig. 14. Schematic illustration of the search algorithm to locate a node n of a new mesh within an element of the new mesh containing the node p closest to n.

$$x_n - \sum_{i=1}^{8} N_i(\xi_n, \eta_n)x_i = 0,$$
$$y_n - \sum_{i=1}^{8} N_i(\xi_n, \eta_n)y_i = 0, \quad (11)$$

where N_i are the shape functions of the 8-noded quadratic isoparametric element. These sets of nonlinear equations are solved using an iterative Newton–Raphson method. The starting guess of the local coordinate ξ_n and η_n is supplied by solving Eq. (11) for a 4-noded linear isoparametric element, which is readily obtained.

Now that the nodes of the new mesh can be located with respect to the elements of the old mesh, the residual stresses from the old mesh are mapped onto the new mesh by inverse isoparametric mapping. Here the stresses at the centroid of the elements of the old mesh are mapped onto the nodes of the new mesh by using the shape functions of the elements.

A numerical experiment is performed in order to ensure and verify that original residual stress field is retained after the residual stress mapping procedure between two different meshes and the subsequent equilibrium calculation in ANSYS. The model is illustrated in Fig. 15. The numerical specimen is loaded to yielding and then unloaded. The residual stresses created are then mapped to a denser mesh with element sizes 0.25 and 0.125 mm, respectively. Fig. 16 shows the original residual stresses (σ_{xx}, σ_{yy} and σ_{xy}) and the residual stresses after mapping. The residual stress generation is carried out with a 0.5 mm element size. These residual stresses are mapped on a linear elastic material model with identical mesh on the integration points and the element centroid, i.e. constant stress at each element. This shows small variation in the residual stress field; ±10% in comparison with the original residual stress field.

7. Validation of incorporation of residual stresses

7.1. Cold expanded hole in aluminium plate

The validation of the residual stress incorporation technique was carried out on cold expanded holes in an aluminium alloy (2024-T351 Al). Pavier et al. [30–32] carried out extensive research on fatigue crack growth from plain and cold expanded holes in aluminium alloys. Cold expansion of holes is widely used in aerospace structures and introduces compressive residual stresses in the vicinity of the hole. These compressive residual stresses prevent fatigue cracks to initiate and grow during cyclic loading [30]. The elastic–plastic 2D plane strain FE simulation of the cold expansion process is carried out in ANSYS by applying a uniform displacement on the hole edge. The FE-model and dimension is illustrated in Fig. 17. The material model used for the linear elastic–plastic analysis was a von-Mises bi-linear kinematic hardening behaviour with elastic modulus of 71.6 GPa, a Poission's ratio of 0.28, yield stress of 375 MPa and tangent modulus 850 MPa ($E_t = E/84$). The FE analysis started with expanding the hole (4% expansion) and removal of the nodal displacements on the hole to simulate the removal of the mandrel and the residual stresses due to the hole expansion are created. Furthermore, external applied stress, $\Delta\sigma_{external} = 0.67^{*}\sigma_{yield}$ (251 MPa), in form of cyclic loading ($R = 0$) is applied to the plate for 10 cycles, see Fig. 18, in order to study redistribution of residual stresses due to external loading. The residual stress mapping procedure was utilized in order to apply the simulated residual stresses after cyclic loading on the linear elastic fracture mechanical FE model with a predefined crack emanating from the cold expanded hole in order to carry out fatigue crack growth analysis.

Fig. 18 shows the tangential and radial residual stresses due to the cold expansion in the crack growth direction. The residual stresses in the tangential direction shows compressive residual stresses in the magnitude of the yield stress. The tangential residual stress will effect the crack growth in the Mode I direction and will decrease K_{eff} ($K_{applied} + K_{residual}$) due to the compressive residual stress, and hence result in crack closure ($K_{eff} < 0$) for external loads less than $\Delta\sigma_{external} = 0.46^{*}\sigma_{yield}$ (160 MPa). Fig. 19 shows the residual stress redistribution due to the crack growth for 0.3, 3 and 8 mm initial crack.

Fig. 20 shows the K_{eff} with and without residual stress predicted using the developed LEFM FCG and residual stress mapping routine. These results are in good agreement with 2D and 3D crack growth simulation carried out by Pavier et al. How-

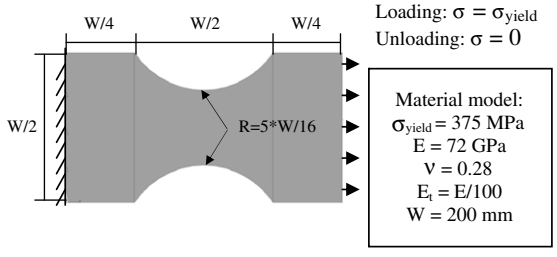

Fig. 15. Numerical model for residual stress mapping study.

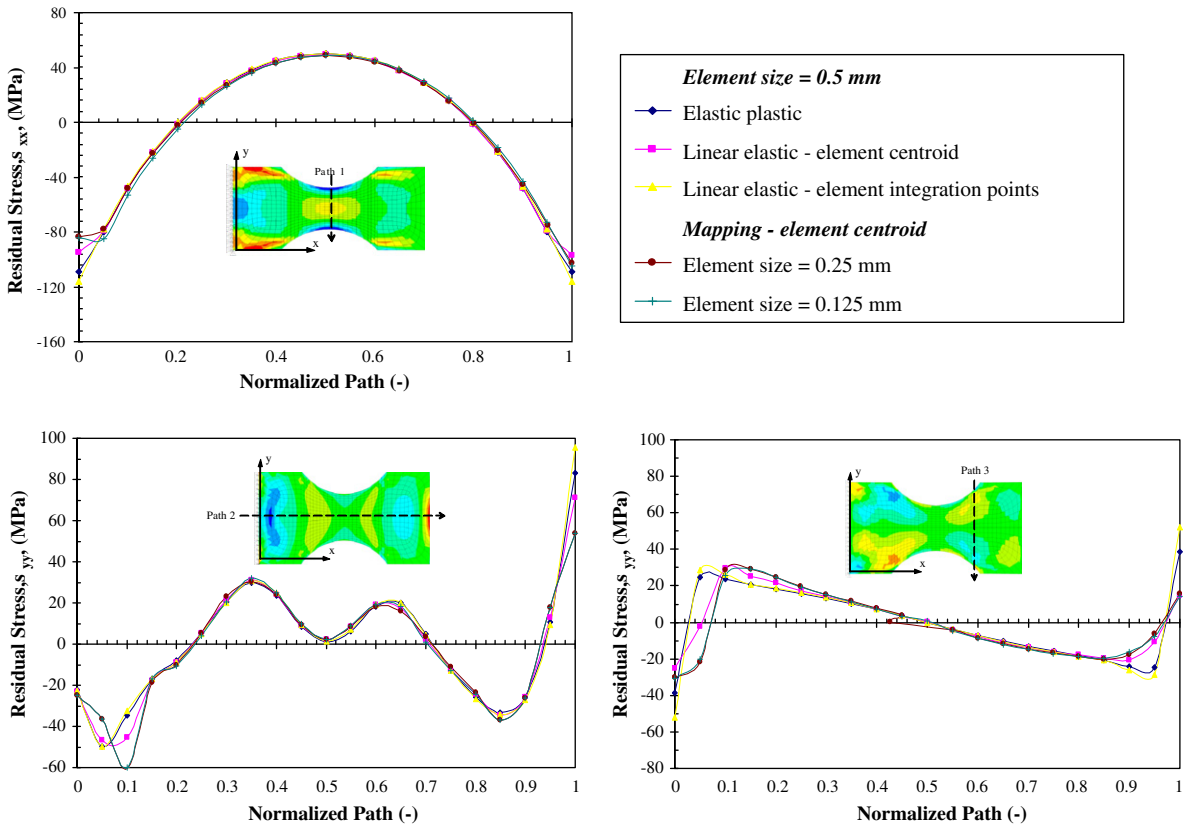

Fig. 16. Residual stresses after mapping to denser mesh and equilibrium calculation using the developed mapping procedure.

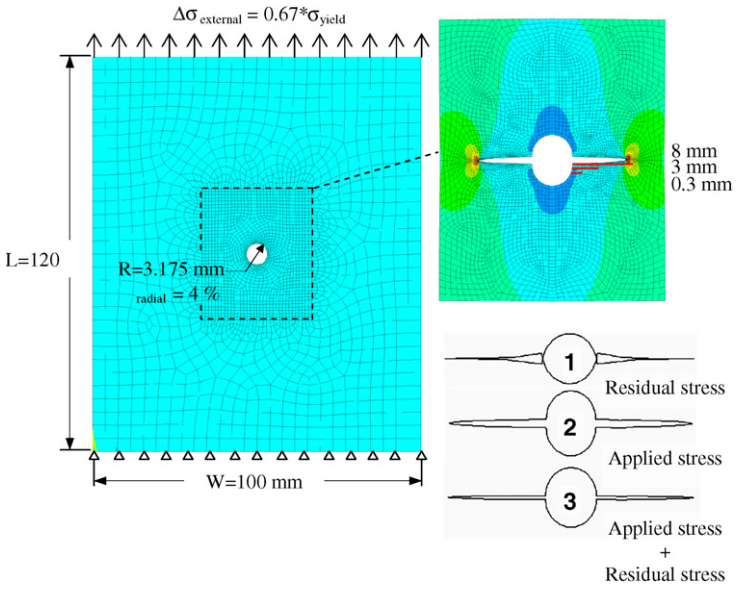

Fig. 17. FE model for cold expanded hole in a plate and FCG.

ever, for longer cracks than 4 mm the predicted results are slightly higher. This is due to the prediction of incremental deflection of the crack during the crack growth implemented in the LEFM FCG routine. This crack deflection is not considered by Pavier et al. [32].

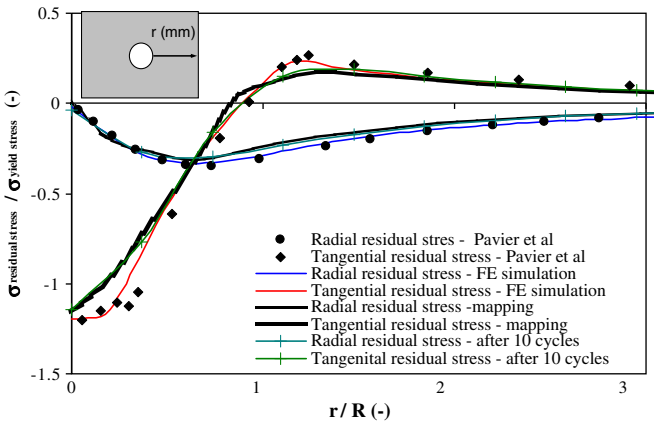

Fig. 18. Predicted residual stresses due to the cold expansion of hole in plate, cyclic loading and residual stress mapping to a LEFM model.

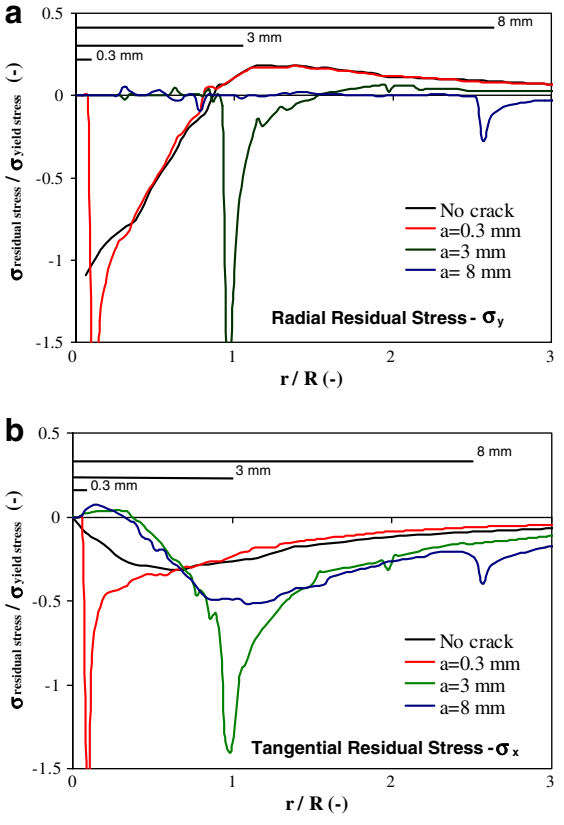

Fig. 19. Relaxation and redistribution of the residual stress during fatigue crack growth in cold expanded hole: (a) radial residual stress and (b) tangential residual stress.

8. Case study: welded diesel engine frame box

The objective of this case study is to carry out welding simulation and LEFM analysis on a welded frame box in a MAN B&W diesel engine. In Hansen and Agerskov [33–34] welding simulations and fatigue testing were carried out on the welded engine part. The welding simulations showed compressive residual stresses in the vicinity of the weld roots. All the fatigue tests failed from the weld root. The stress relieving by PWHT (post-weld heat treatment) reduced the fatigue resistance due to the relieving of the beneficial compressive residual stresses at weld root. For further details see Hansen and Agerskov [33–34]. Fig. 21 illustrates the large two stroke diesel engine and the welded frame box analyzed.

Please cite this article in press as: Barsoum Z, Barsoum I, Residual stress effects on fatigue life of welded structures using LEFM, Eng Fail Anal (2008), doi:10.1016/j.engfailanal.2008.06.017

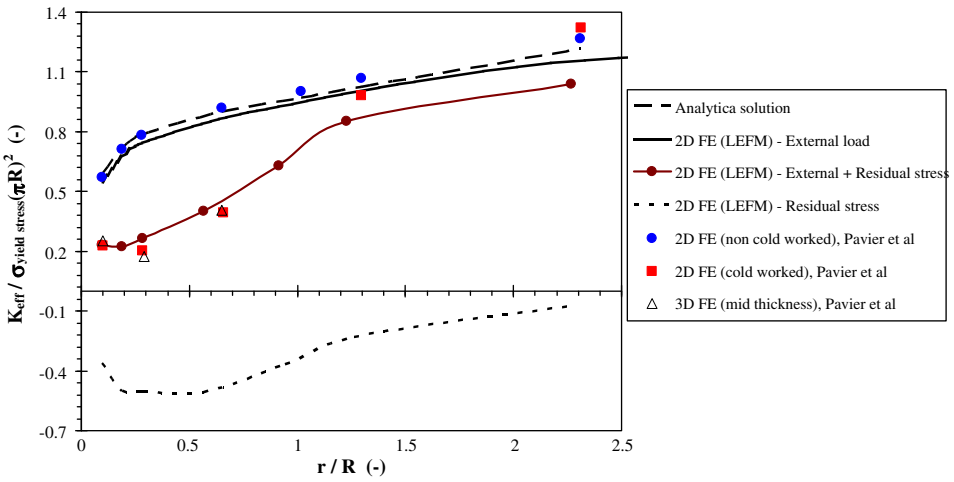

Fig. 20. Effective stress intensity factor as function of crack length, including the effects of residual stresses

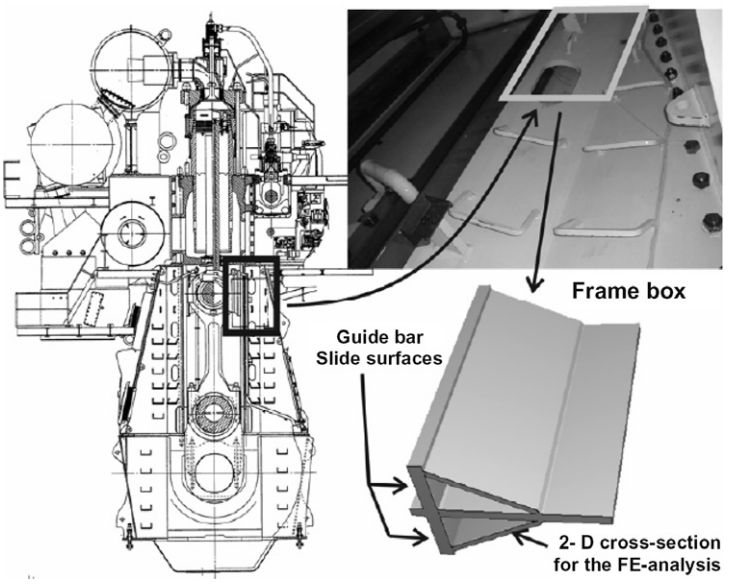

Fig. 21. Two stroke diesel engine and welded frame box part analysed.

Martinsson [9] carried out fatigue life prediction on the welded diesel engine frame box. However, crack propagation analysis incorporating welding residual stress and their redistribution and incremental crack path deflection analysis was not incorporated in the LEFM model by Martinsson [9].

8.1. Welding simulation and residual stress prediction

The welding simulation was carried out using the developed welding simulation procedure. The engine frame box is welded with two welds, weld A and weld B, and each weld with four passes, respectively. For the non-penetrated root (5 mm for weld A and 8 mm for weld B) contact element were used in order to prevent penetration of the main plates during the welding simulation. Fig. 22 shows the FE mesh and dimensions. Fig. 23 shows the predicted temperature results from the thermal analysis. The residual stress prediction results are in general in qualitative good agreement with the measurement carried out in Hansen [33]. However, the measurements show systematically lower stresses due to a cutting operation before the measurements which resulted in a considerable residual stress relaxation [35]. Fig. 24 shows the predicted residual stresses at the specified locations of the measurement positions. Details about, i.e. welding procedure are not reported here and are outlined in Hansen [33]. The predicted residual stresses in the normal direction of the assumed crack path are shown

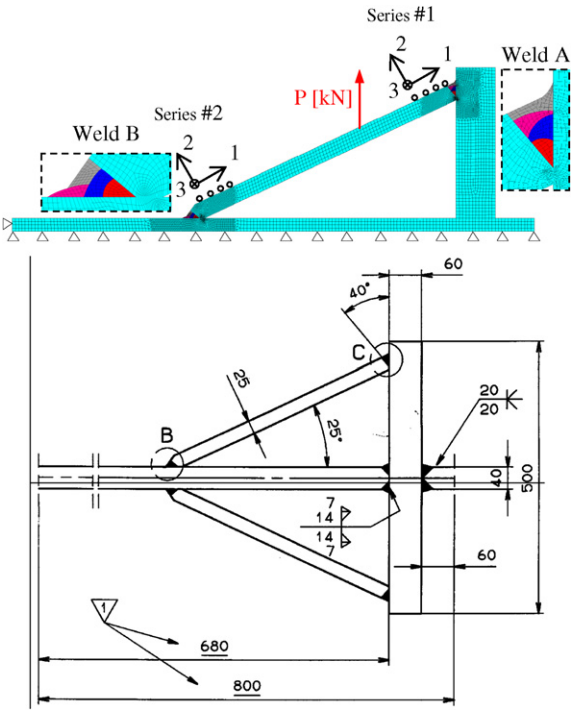

Fig. 22. Welding simulation of engine frame box: FEM mesh, welds, dimensions and remote loading during fatigue testing.

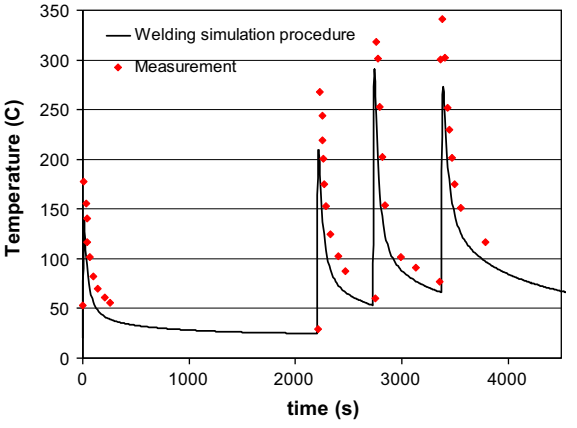

Fig. 23. Temperature predictions.

in Fig. 25 for weld A and B, respectively. It can be seen that the weld root gaps are under favourable compressive residual stresses.

8.2. Fatigue life prediction

The fatigue testing of the welded diesel engine frame box is well documented in Hansen and Agerskov [28]. The fatigue testing was carried out in constant amplitude loading with $R = 0$ on 90 mm cut out test pieces. A set of the welded components were stress relieved by post-weld heat treatment (PWHT) before fatigue testing. The compressive residual stress is relieved with PWHT and is clearly seen in the predicted Fig. 26, where the predicted and experimentally fatigue lives are compared. The fatigue life predictions for the PWHT specimens show good agreement with experiments. The threshold value (ΔK_{th}) is predicted to 5.98 MPa $\sqrt{m}$. Hobbacher [18] states a conservative regression curve for structural C-and CM-steels in for the threshold value with $K_{th} = 6$ MPa $\sqrt{m}$ at external $R = 0$. The suggestion is

Please cite this article in press as: Barsoum Z, Barsoum I, Residual stress effects on fatigue life of welded structures using LEFM, Eng Fail Anal (2008), doi:10.1016/j.engfailanal.2008.06.017

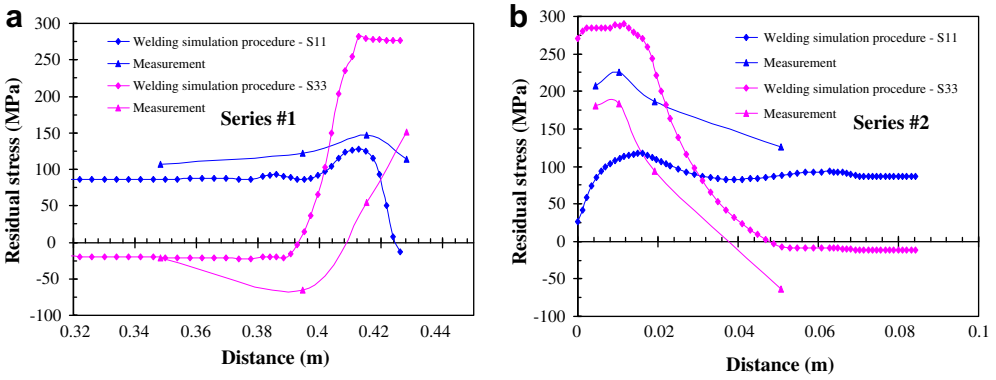

Fig. 24. Predicted residual stresses for engine frame box.

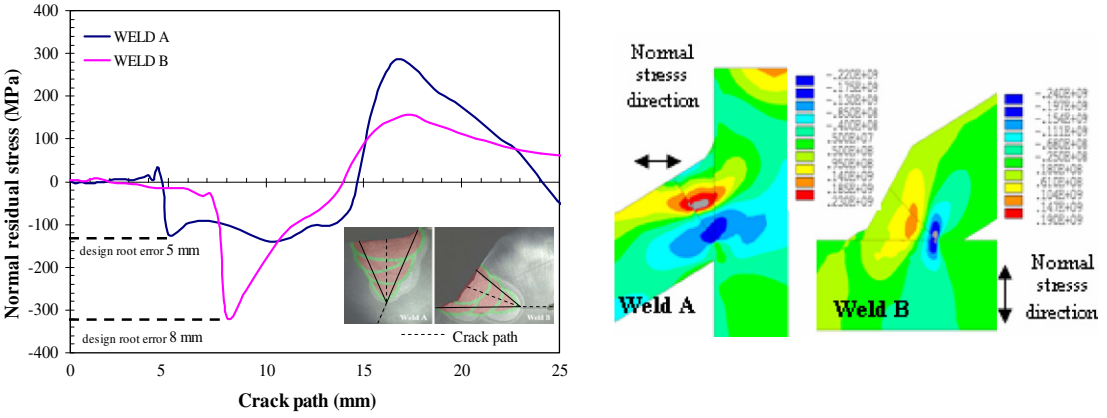

Fig. 25. Predicted residual stresses along the root and trough the weld in the normal direction of the assumed crack path.

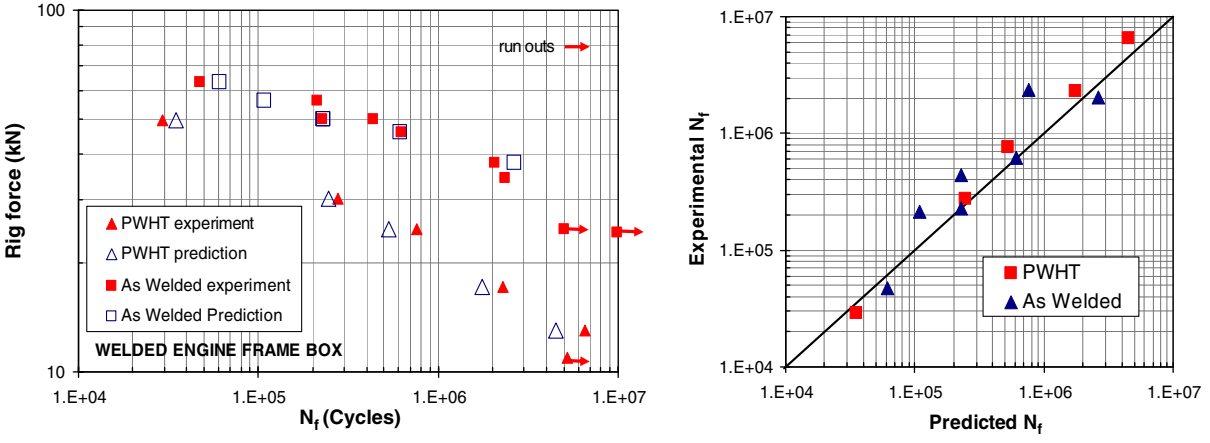

Fig. 26. Welded engine frame box, fatigue life prediction.

$$\Delta K_{th} = 6.0 - 4.6 \cdot R. \tag{12}$$

In Table 1 the initial K-values for the initial root crack defects are summarized for weld A and weld B, respectively. The root crack in weld B is under compression and will remain closed for the as welded specimens, consequently all the specimens, as welded and PWHT, failed from weld A from the weld root.

Please cite this article in press as: Barsoum Z, Barsoum I, Residual stress effects on fatigue life of welded structures using LEFM, Eng Fail Anal (2008), doi:10.1016/j.engfailanal.2008.06.017

Table 1
Predicted threshold values in (MPa $\sqrt{m}$)

	As welded		PWHT	
	Weld A	Weld B	Weld A	Weld B
$K_{I,\ res}$	−2.3	−15	–	–
$K_{I,\ applied}$ (min)	13.05	6.8	5.98	3.1
K_I	10.75	−8.2	5.98	3.1
a_{inital} (mm)	5	8	5	8
$\Delta K_{I,\ threshold}$	10.75 (24 kN)	– (46 kN)	5.98 (11 kN)	– (21 kN)

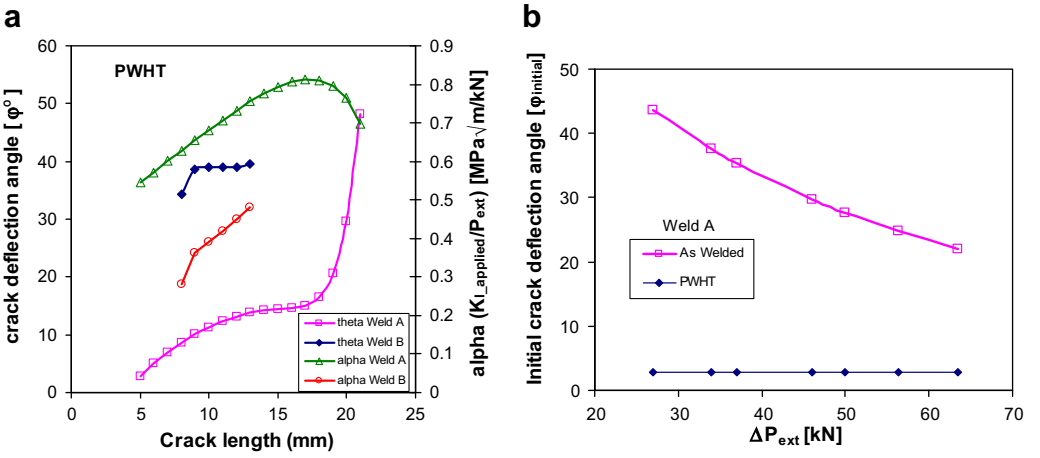

Fig. 27. Welded engine frame box: (a) crack deflection angle as function of crack length for PWHT weld A and B and (b) initial crack deflection for weld A.

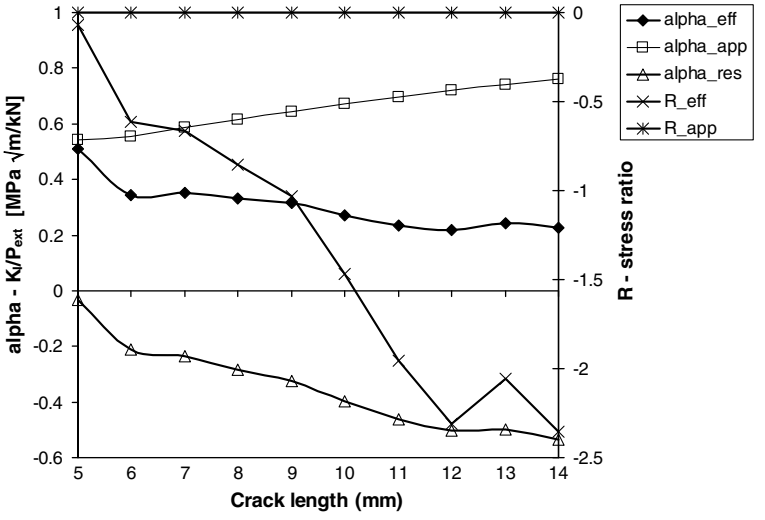

Fig. 28. Welded engine frame box, weld A. Predicted K_I due to applied loading and residual stress along the crack path, R_{eff} and R_{app}. K_I normalized with applied loading.

In Fig. 27a the predicted crack deflection angle (φ) is plotted against the crack length for PWHT (no residual stresses) specimens for weld A and B, respectively. The crack deflection is increasing for the growing root crack in weld A with increasing crack growth and ΔK_I. However, the initial crack deflection angle in weld A is affected by the presence of residual stress and different magnitude of external loading; hence increase of ΔP_{ext} will decrease $\varphi_{initial}$ as can be seen in Fig. 27b. In Fig. 28 the stress intensity factor due to applied loading ($K_{I,applied}$), residual stress ($K_{I,res}$) and effective ($K_{I,eff}$) is normalized with applied loading ΔP_{ext} and plotted as a function of crack length. It can be noted that the presence of compressive residual stress will considerably decrease the effective K_I. The effective R-ratio and the applied R-ratio (0) is also plotted in Fig. 28.

Please cite this article in press as: Barsoum Z, Barsoum I, Residual stress effects on fatigue life of welded structures using LEFM, Eng Fail Anal (2008), doi:10.1016/j.engfailanal.2008.06.017

9. Conclusions

A FE welding simulation procedure is developed in order to predict the residual stress due to welding. The predicted residual stresses mapped on the developed LEFM fatigue crack growth model in order to study the interaction between residual stresses and external fatigue loading. The models are used to predict the fatigue life of weld defects. The following conclusions are made:

1. The residual stress prediction shows good agreement with data found in the literature, i.e. for residual stresses in fillet welds. However, the transverse residual stress in butt welds shows poor agreement with measurements. This is mostly due to 3D effect of welding; a 3D model is subjected to larger constraint than a 2D model and this will result in higher transverse stresses.
2. The predicted residual stresses and effective stress intensity factors in the validation example shows good agreement with the results found in the literature. The residual stress redistribution due to crack growth is predicted with reasonable accuracy by the LEFM fatigue crack growth routine and the residual stress mapping routine. However, the predicted K_{eff} for cracks larger than 4 mm are slightly conservative. This is due to the incorporation of the crack deflection during each crack growth increment in the LEFM model.
3. The residual stress predictions for the analyzed case study, welded engine frame box, shows principally good agreement with measurements. Compressive residual stresses are found at weld roots which will enhance the fatigue life. The fatigue life prediction using the developed LEFM subroutine and the mapping procedure confirms the fatigue life enhancement for the as welded specimens compared with the stress relived. However, at high fatigue lives the predictions are non-conservative. This is due to the magnitude of the predicted residual stresses is non-conservative. There is an effect of the residual stress on the crack deflection angle and the true R-ratio; R_{eff}.

Acknowledgements

Dr. Jan Langkjaer Hansen at MAN B&W is acknowledged for valuable discussions. Professor Dan Zenkert and Professor Mårten Olsson at Kungliga Tekniska Högskolan and Professor Lars-Erik Lindgren at Luleå University of Technology are acknowledged for reading trough the manuscript and contributed with valuable discussion and comments.

References

[1] Martinsson J. Comparisons between different contemporary FCG programs on welded components. IIW Document, No. XIII-1994-03, 2003.
[2] Finch D, Burdekin FM. Effect of welding residual stress on significance of defects in various types of welded joints. Eng Fract Mech 1992;41(5):721–35.
[3] AFGROW. Version 4.0005. <http://fibec.flight.wpafb.af.mil/fibec/afgrow.html>.
[4] Lindgren L-E. Finite element modelling and simulation of welding, Part1: increasing complexity. J Therm Stresses 2001;24:141–92.
[5] Lindgren L-E. Finite element modelling and simulation of welding, Part2: improved material modelling. J Therm Stresses 2001;24:195–231.
[6] Lindgren L-E. Finite element modelling and simulation of welding, Part3: efficiency and integration. J Therm Stresses 2001;24:305–34.
[7] FRANC2D. Version 3.2. <http://www.cfg.cornell.edu/>.
[8] Bittencourt TN, Wawrzynek PA, Ingraffea AR, Sousa JL. Quasi-automatic simulation of crack propagation for 2D LEFM problems. Eng Fract Mech 1996;55(2):321–34.
[9] Martinsson J. Fatigue assessment of complex welded steel structures. Doctoral Thesis, Department of Aeronautical and Vehicle Engineering, KTH, Sweden, 2005. ISBN 91-2783-968-6.
[10] Finch D, Burdekin FM. Effect of welding residual stress on significance of defects in various types of welded joints – II. Eng Fract Mech 1992;42(3):479–500.
[11] Michaleris P, Kirk M, Mohr W, McGaughy T. Incorporation of residual stress effects into fracture assessment via the finite element method. In: Underwood JH, Macdonald BD, Mitchell MR, editors. Fatigue and fracture mechanics. ASTM STP 1321 1997;vol. 28. American Society for Testing and Materials; 1997.
[12] Stacey A, Barthelemy J-Y, Leggatt RH, Ainsworth RA. Incorporation of residual stresses into the SINTAP defect assessment procedure. Eng Fract Mech 2000;67:573–611.
[13] ANSYS guide. ANSYS release 10.0. Swanson Analysis Systems: Houston.
[14] Radaj D. Heat effects of welding. Berlin: Springer-Verlag; 1992.
[15] Hong JK, Tsai CL, Dong P. Assessment of numerical procedures for residual stress analysis of multi-pass welds. Weld Res Suppl 1998:372–82.
[16] MatWeb. Online materials information resource. <http://www.matweb.com/>.
[17] Andersson B. Thermal stresses in a submerged-arc welded joint considering phase transformations. J Eng Mater Technol 1978;100:356–62.
[18] Radaj D. Welding residual stresses and distortion. Berlin: Springer-Verlag; 2003.
[19] Hansen JL. Numerical modeling of welding induced stresses. PhD thesis, Technical University of Denmark. ISBN 87-90855-52-3, 2003.
[20] Goldak J. Personal communication. Department of Mechanical and Aerospace Engineering, Carleton University, Ottawa, ON K1S 5B6, Canada.
[21] Dong P, Zhang J. Residual stresses in strength mismatched welds and implications on fracture behaviour. Eng Fract Mech 1999;64:485–505.
[22] Ma N-X, Ueda Y, Murakawa H, Maeda H. FEM analysis of 3D welding residual stresses and angular distortion in T-type fillet welds. Trans Jpn Weld Res Inst 1995;24(2):115–22.
[23] Erdogan F, Sih GC. On the crack extension in plates under plane loading and transverse shear. ASME J Basic Eng 1963;85:519–27.
[24] Hussain MA, Pu SL, Underwood JH. Strain energy release rate for a crack under combined mode I and II. ASTM STP 560, 1974. p. 2–28
[25] Sih GC. Strain energy density factor applied to mixed mode crack problems. Int J Fract Mech 1974;10:305–21.
[26] Hobbacher A. Recommendations for fatigue design of welded joints and components. IIW document XIII-1965-03/XV-1127-03, 2003.
[27] Edwards L. Influence of residual stress redistribution on fatigue crack growth and damage tolerant design. Mater Sci Forum 2006;524–525:363–72.
[28] Dowling NE. Mechanical behaviour of materials: engineering methods for deformation fracture and fatigue. 2nd ed. Prentice-Hall; 1999.
[29] Benson DJ. Computational methods in Lagrangian and Eulerian hydrocodes. Comput Methods Appl Mech Eng 1992;99(2):235–394.
[30] Lacarac VD, Garcia-Granada AA, Smith DJ, Pavier MJ. Prediction of the growth rate for fatigue cracks emanating from cold expanded holes. Int J Fatigue 2004;26(6):585–95.

Please cite this article in press as: Barsoum Z, Barsoum I, Residual stress effects on fatigue life of welded structures using LEFM, Eng Fail Anal (2008), doi:10.1016/j.engfailanal.2008.06.017

[31] Lacarac VD, Smith DJ, Pavier MJ, Priest M. Fatigue crack growth from plain and cold expanded holes in aluminium alloys. Int J Fatigue 2000;22(3):189–203.
[32] Pavier MJ, Poussard CGC, Smith DJ. Effect of residual stress around cold worked holes on fracture under superimposed mechanical load. Eng Fract Mech 1999;63(6):751–73.
[33] Hansen JL. Residual stress from welding of large diesel engine structures. In: Samulesson J, editor. Design and analysis of welded high strength steel structures. Stockholm: EMAS; 2002. p. 345–72.
[34] Hansen JL, Agerskov H. Fatigue assessment of root defects in the welded structure of a diesel engine. In: Samulesson J, editor. Design and analysis of welded high strength steel structures. Stockholm: EMAS; 2002. p. 373–90.
[35] Hansen JL. Personal communication. MAN B&W Diesel, Copenhagen, Denmark.

Please cite this article in press as: Barsoum Z, Barsoum I, Residual stress effects on fatigue life of welded structures using LEFM, Eng Fail Anal (2008), doi:10.1016/j.engfailanal.2008.06.017